Reviews in Mineralogy & Geochemistry
Vol. 71 pp. 299-314, 2010

Multi-Mbar Phase Transitions in Minerals

Koichiro Umemoto

Department of Geology and Geophysics
University of Minnesota
Minneapolis, Minnesota, 55455, U.S.A.

umemoto@cems.umn.edu

Renata M. Wentzcovitch

Department of Chemical Engineering and Materials Sciences and
Minnesota Supercomputer Institute, University of Minnesota
Minneapolis, Minnesota, 55455, U.S.A.

wentzcov@cems.umn.edu

INTRODUCTION

$MgSiO_3$ perovskite is the most abundant mineral in the Earth's lower mantle. A structural phase transition in this phase to a $CaIrO_3$-type polymorph was discovered in 2004 (Murakami et al. 2004; Oganov and Ono 2004; Tsuchiya et al. 2004). This new polymorph, the so-called post-perovskite (PPV) phase, was produced at pressures and temperatures close to those expected at the core-mantle boundary, 125 GPa and 2,500 K (Murakami et al. 2004). In the Earth, the PPV phase is the final form of $MgSiO_3$. This surprising discovery invited a new question: what is the next polymorph of $MgSiO_3$? $MgSiO_3$ PPV consists of SiO_3 layers intercalated by magnesium (Fig. 1). Therefore, it is natural to expect still other pressure induced transitions to more isotropic close-packed looking structures. This question has acquired further importance since the discovery of terrestrial-type exoplanets: the Super-Earth planet with ~7 Earth masses, GJ876d (Rivera et al. 2005), and the Saturn-like planet with a massive dense core with ~67 Earth masses, D149026b (a dense-Saturn) (Sato et al. 2005). Many others have been found since then. Pressures and temperatures in the mantle of these planets are much higher than in the Earth. There is also a pressing need to understand and model matter in the core of the giants, particularly the solar ones, Jupiter, Saturn, Uranus, and Neptune. In GJ876d, pressure and temperature at its core-mantle boundary was roughly estimated to be ~1 TPa (10 Mbar) and ~4,000 K (Valencia et al. 2006). The gas giants, Jupiter and Saturn, and the icy giants, Uranus and Neptune, have small dense cores surrounded by hydrogen/helium and ice, respectively. Pressures and temperatures at the core-envelope boundaries of these planets have been estimated to be 40 Mbar and 15,000~20,000 K in Jupiter, 10 Mbar and 8,500~10,000 K in Saturn, 8 Mbar and ~8,000 K in Uranus and Neptune (Guillot 2004). To improve modeling of their interiors, there should be a better understanding of possible

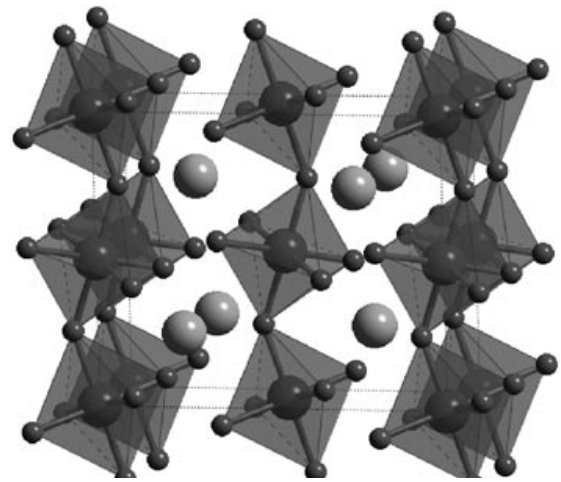

Figure 1. Structure of $MgSiO_3$ post-perovskite (PPV).

1529-6466/10/0071-0014$05.00 DOI: 10.2138/rmg.2010.71.14

phases ($MgSiO_3$ PPV, etc.) and their equations of state under these extreme conditions. Experimentally, it is very challenging to achieve such extremely high pressures and temperatures. The National Ignition Facility (NIF), expected to enter in operation in 2010, offers hope for some data on materials at these conditions. However, first-principles computational methods are very powerful and promising to investigate materials properties at these extreme conditions. They are forging ahead and making predictions to be tested at NIF in the 10^2 Mbar and 10^5 K regime (Umemoto et al. 2006a; Wu et al. 2008; Sun et al. 2008; Umemoto et al. 2008).

In this paper, we discuss first-principles investigations of post-PPV transitions in planet-forming minerals, $MgSiO_3$ and Al_2O_3, at multi-Mbar pressures. We will also discuss low-pressure analogs of these minerals. They can provide experimentally convenient alternatives for exploration of post-PPV transitions. We will see a close relationship between the multi-Mbar chemistry of planet-forming minerals and those of rare-earth sesquisulfides and transition-metal sesquioxides.

COMPUTATIONAL BACKGROUND

This section briefly describes these first principles density functional theory (DFT) (Hohenberg and Kohn 1964; Kohn and Sham 1965) calculations. DFT makes use of approximations for the exchange-correlation (XC) energy. Several XC energy functionals exist, but the most widely used are based on the local-density approximation (LDA) (Ceperley and Alder 1980; Perdew and Zunger 1981) and on the generalized density approximation (GGA), in particular the PBE functional (Perdew et al. 1996). They have been successfully used for many minerals (Wentzcovitch et al. 2010, in this volume). PBE-GGA is also relatively successful for calculations in H_2O-ice. Wave functions are expanded in plane waves in combination with pseudopotentials (Vanderbilt 1990). At multi-Mbar pressures, care must be exercised when generating pseudopotentials. Inter-atomic distances become very small at these extreme pressures, and pseudopotential cut-off radii must be sufficiently small to avoid core overlap. It is often necessary to promote semi-core state to valence. In Umemoto et al. (2006a), 2*s* and 2*p* states of silicon, usually treated as core states, were promoted to valence states. Using the plane wave pseudopotential method, total energy, forces, and stress are efficiently evaluated. Structural search and optimizations are performed at arbitrary pressures using a damped form of variable-cell-shape molecular dynamics (Wentzcovitch 1991; Wentzcovitch et al. 1993). The dynamical stability of optimized structures is assessed by calculation of phonon frequencies. These are calculated by diagonalizing the dynamical matrices obtained using density-functional perturbation theory (Giannozzi et al. 1991; Baroni et al. 2001). The system is dynamically stable if all phonon frequencies are real throughout the Brillouin zone. Phonon frequencies are also used to calculate the Helmholtz free energy within the quasi-harmonic approximation (QHA) (Wallace 1972). All thermodynamic properties, including Gibbs free energies at arbitrary pressures and temperatures, can then be obtained. Knowledge of the Gibbs free energies of two or more phases, phase transformations can be investigated.

DISSOCIATION OF $MgSiO_3$ PPV

The first prediction of a post-PPV transition was the dissociation of $MgSiO_3$ (Umemoto et al. 2006a) into CsCl-type MgO and cotunnite-type SiO_2 at 1.12 TPa (11.2 Mbar) in static enthalpy calculations (Fig. 2). CsCl-type MgO and cotunnite-type SiO_2 have not been synthesized experimentally yet, but they are the most probable candidates of high-pressure forms of MgO and SiO_2 in the dissociation pressure range. The calculated phase boundary shown in Figure 3 indicates that $MgSiO_3$ PPV should not exist any longer in the cores of the gas giants (Jupiter and Saturn) but could survive in cores of the icy giants (Uranus and Neptune). This transition may occur in the mantles of Super-Earths-type exoplanets (Rivera et

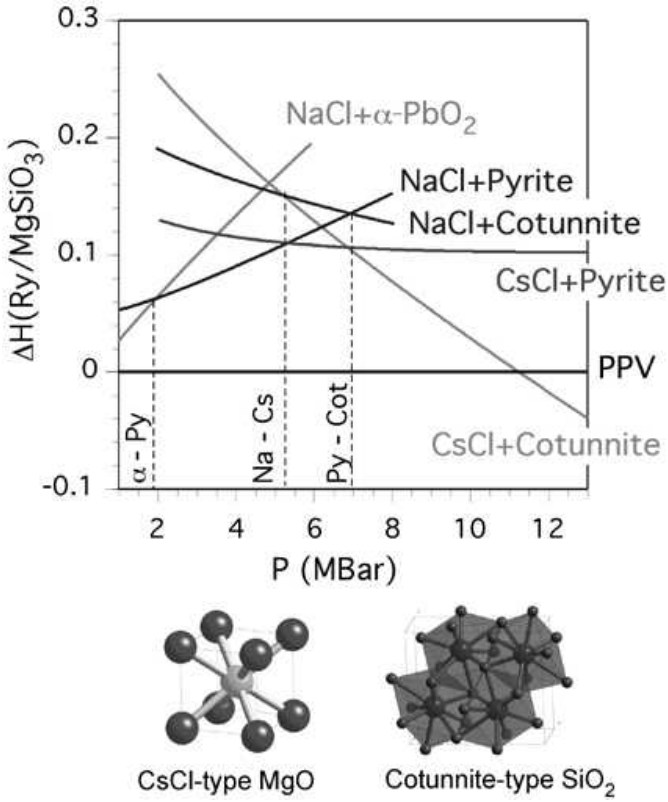

Figure 2. Static enthalpies of aggregation of MgO and SiO_2 in various forms with respect to that of $MgSiO_3$ PPV (Umemoto et al. 2006a). Vertical dashed lines denote static transition pressures of NaCl-type—CsCl-type MgO (5.3 Mbar), a-PbO_2-type—Pyrite-type SiO_2 (1.9 Mbar), and Pyrite-type—cotunnie-type SiO_2 (6.9 Mbar). These values are consistent with those of other calculations (Mehl et al. 1988; Oganov et al. 2003; Oganov et al. 2005).

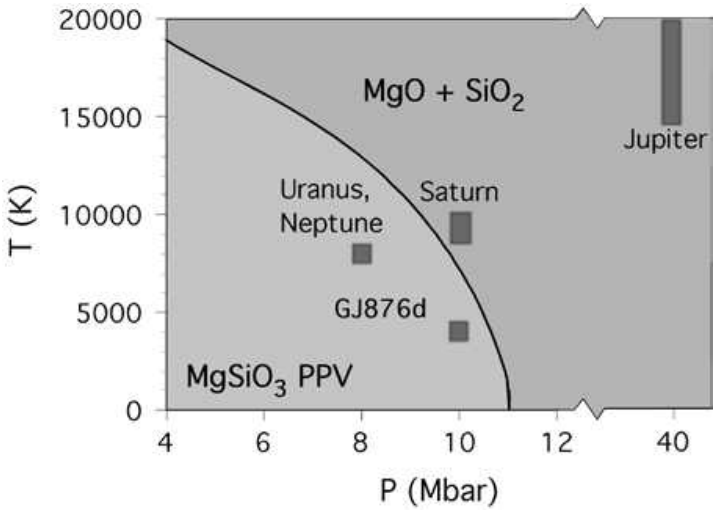

Figure 3. Dissociation phase boundary in $MgSiO_3$. PPV is predicted to dissociate into CsCl-type MgO and cotunnite-type SiO_2. Rectangles denote estimated pressure-temperature conditions at core-envelope boundaries in the solar giants and in GJ876d.

al. 2005), depending on their masses and temperatures, and in dense larger exoplanets (Sato et al. 2005). Along the dissociation phase boundary the mixture of products was found to be denser than the PPV phase by 1~3%, depending on temperature. The coordination number of silicon increases from 6 to 9 and the averaged bond lengths increase as well. This lowers the vibrational entropy of the dissociation products. Consequently, the Clapeyron slope for this transition is negative. In GJ876d, the dissociation is likely to occur near its CMB (Valencia et al., 2006). The eventual occurrence of this endothermic transition with a large negative Clapeyron slope would be equivalent to the occurrence of the endothermic post-spinel transition near the core of Mars. Geodynamical modeling suggests that this might be the cause of a proposed large martian superplume (Weinstein 1995). Convection in D149026b (Sato et al. 2005), where internal pressures and temperatures should be much higher than in Saturn,

could be dramatically affected. A transformation with such large negative Clapeyron slope in the middle of its silicate core-mantle is likely to inhibit convection (Tackley 1995), promote layering, and produce a differentiated core-mantle, with the bottom layer consisting primarily of oxides. Thermal excitation of carriers at the high temperatures relevant for the solar giants and exoplanets affects noticeably important mineral properties. Finite electronic temperature (Mermin 1965; Wentzcovitch et al. 1992) calculations indicated that although the dissociation products are intrinsic semiconductors with electronic band gaps, the carrier concentrations in cotunnite-type SiO_2 become typical of semimetals or heavily-doped semiconductors at 1 TPa and 10,000~20,000 K (Umemoto et al. 2006a). Hence these minerals can be seen essentially as metals with rather high electric and thermal conductivities. This is important information for improving models of the solar giants' interiors and of terrestrial exopolanets.

LOW-PRESSURE ANALOG OF $MgSiO_3$

Although the dissociation of $MgSiO_3$ should be important for the solar giants and terrestrial exoplanets, the predicted dissociation pressure is still too high to be achieved routinely by experiments (~1 TPa). Therefore, low-pressure analogs of $MgSiO_3$ are highly desirable for experimental investigations of properties of the $CaIrO_3$-type structure, including its dissociation. In general, analog compounds with the same structure and larger ions tend to have lower transition pressures. Atomic/ionic sizes increase downwards and towards the left in the periodic table. There are several candidates for low-pressure analogs of $MgSiO_3$, e.g., $CaIrO_3$ (Hirose and Fujita 2005; Tsuchiya and Tsuchiya 2007), $MgGeO_3$ (Ross and Navrotsky 1988; Hirose et al. 2005; Kubo et al. 2006, 2008), Mn_2O_3 (Santillán et al. 2006), and $NaMgF_3$ (Liu et al. 2005; Hustoft et al. 2008). Among them, $NaMgF_3$ (neighborite) is one of the best candidates. It is a stable *Pbnm* perovskite phase at ambient conditions and undergoes a pressure-induced phase transition to the $CaIrO_3$-type phase (Liu et al. 2005; Hustoft et al. 2008). Umemoto et al. (2006b) predicted by first principles that $NaMgF_3$ has qualitatively the same phase diagram as $MgSiO_3$: the PPV transition has a positive Clapeyron slope and the PPV dissociation into CsCl-type NaF and cotunnite-type MgF_2 has a negative Clapeyron slope (Umemoto et al. 2006b). NaF and MgF_2 are also low-pressure analogs of MgO and SiO_2 (Yagi et al. 1983; Haines et al. 2001). The dissociation pressure in $NaMgF_3$ occurs at ~40 GPa (Fig. 4), which is much lower than that of $MgSiO_3$ and can be easily achieved by static compression

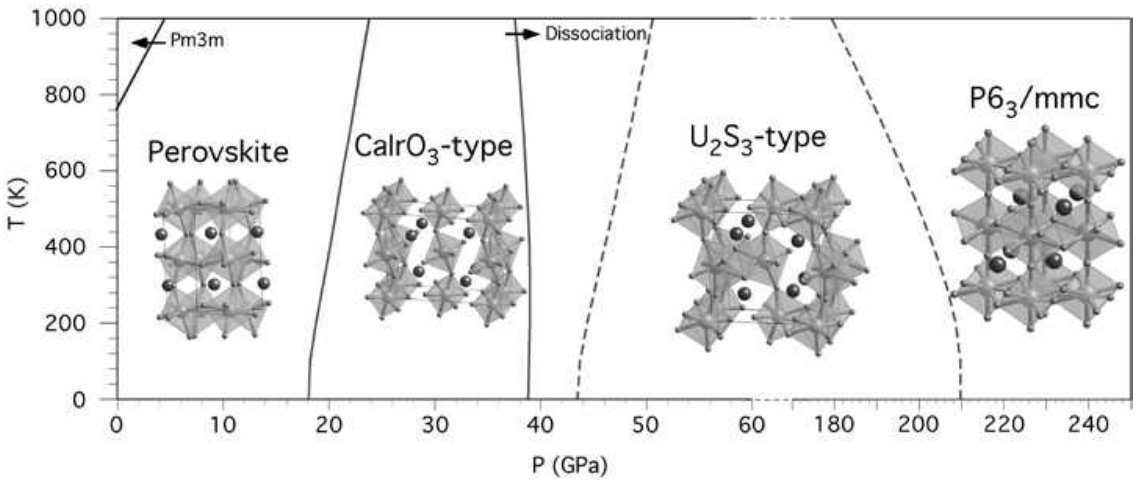

Figure 4. Calculated phase boundaries of $NaMgF_3$ (Umemoto and Wentzcovitch 2006). Two dashed lines denote the metastable phase boundaries between $CaIrO_3$-type and U_2S_3-type, and between U_2S_3-type and $P6_3/mmc$ phases, respectively. The solid line in the upper left corner denotes the experimental phase boundary between orthorhombic perovskite and cubic phases (Zhao et al. 1994).

experiments. Therefore, $NaMgF_3$ should be a good low-pressure analog of $MgSiO_3$ to test the possibility of a dissociation transition. The PPV transition and subsequent dissociation have also been predicted in $CaSnO_3$ (Tsuchiya and Tsuchiya 2006). Despite the latter being an oxide compound, its dissociation pressure was found to be ~70 GPa, which is also quite low compared to that in $MgSiO_3$.

PREDICTION OF POST-PPV CRYSTALLINE PHASES

Although the dissociations of $MgSiO_3$, $NaMgF_3$, and $CaSnO_3$ PPV were predicted, it is not guaranteed that all ABX_3 PPVs should dissociate. Some of them might prefer to undergo a post-PPV transition to another ABX_3 polymorph before dissociating. What could happen if the dissociation is inhibited? Umemoto and Wentzocivtch (2006) investigated the metastable compression of $CaIrO_3$-type $NaMgF_3$ beyond the predicted dissociation pressure (~40 GPa). Up to ~80 GPa, all lattice constants of the $CaIrO_3$-type $NaMgF_3$ decreased as usual. However, there were two anomalies in the behavior of the lattice constants under pressure: increases in lattice constants *a* and *c* at 80 GPa and an abrupt jump of all lattice constants at 150 GPa (Fig. 5). The first anomaly is related to the softening of an acoustic mode at the zone-edge *Y* point (Fig. 6). After superposing the atomic displacements of this particular soft mode to the structure followed by structural re-optimization, new bonds appeared between magnesium and fluorine in adjacent layers. This resulted in a phase transformation from the $CaIrO_3$-type phase to a phase with *Pmcn* symmetry (the *Pnma* symmetry in the standard setting), a sub-group of *Cmcm*. This phase is isostructural with U_2S_3 (Fig. 7b). The magnesium coordination number is 7, larger than that of the $CaIrO_3$-type phase, 6. A possible crystallographic relationship between the $CaIrO_3$-type and the U_2S_3-type structures was discussed by Hyde et al. (1979). It is interesting to note that $UFeS_3$ has the $CaIrO_3$-type structure. Replacement of iron by uranium leads to the U_2S_3-type structure. The second anomaly corresponds to an increase in symmetry of the $CaIrO_3$-type phase and generates a new phase with $P6_3/mmc$ symmetry, a super-group of *Cmcm* (Fig. 7c). The magnesium coordination number in this phase is 8, higher than 6 in the $CaIrO_3$-type and 7 in the U_2S_3-type phases. The structural unit is no longer the MgF_6 octahedron but an MgF_8 parallelepiped. Parallelepipeds share edges to form layers in the *ab* plane. Each layer contacts the adjacent ones at the parallelepipeds' apices along the [0001] direction. Sodium is located in interstitial sites between the MgF_8 parallelepipeds. The sodium coordination number is 11. Sodium and magnesium stack in an ABAC sequence (A: magnesium and B, C: sodium), i.e., the sub-lattice formed by sodium and magnesium has the NiAs structure. The sodium and fluorine sub-lattices have the $IrAl_3$–type structure (Hyde and Andersson 1989). As far as we know, the $P6_3/mmc$ phase has not been identified in any material experimentally so far. Both U_2S_3-type and $P6_3/mmc$ phases are dynamically stable phases of $NaMgF_3$. Therefore, these structures are two potential candidates

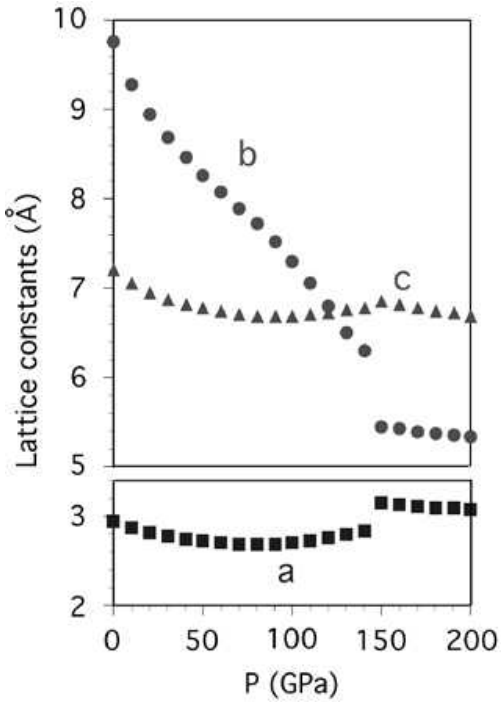

Figure 5. Pressure dependence of calculated lattice constants of $CaIrO_3$-type $NaMgF_3$ (Umemoto and Wentzcovitch 2006).

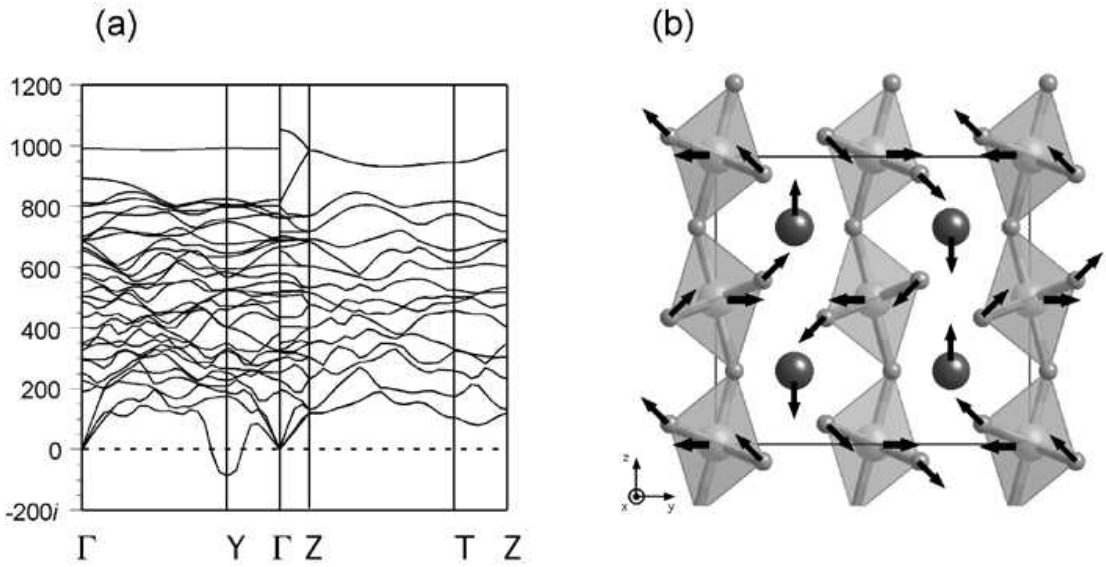

Figure 6. (a) Phonon dispersion of $CaIrO_3$-type $NaMgF_3$ at 100 GPa. (b) Atomic displacements resulting from the unstable phonon at the Y point.

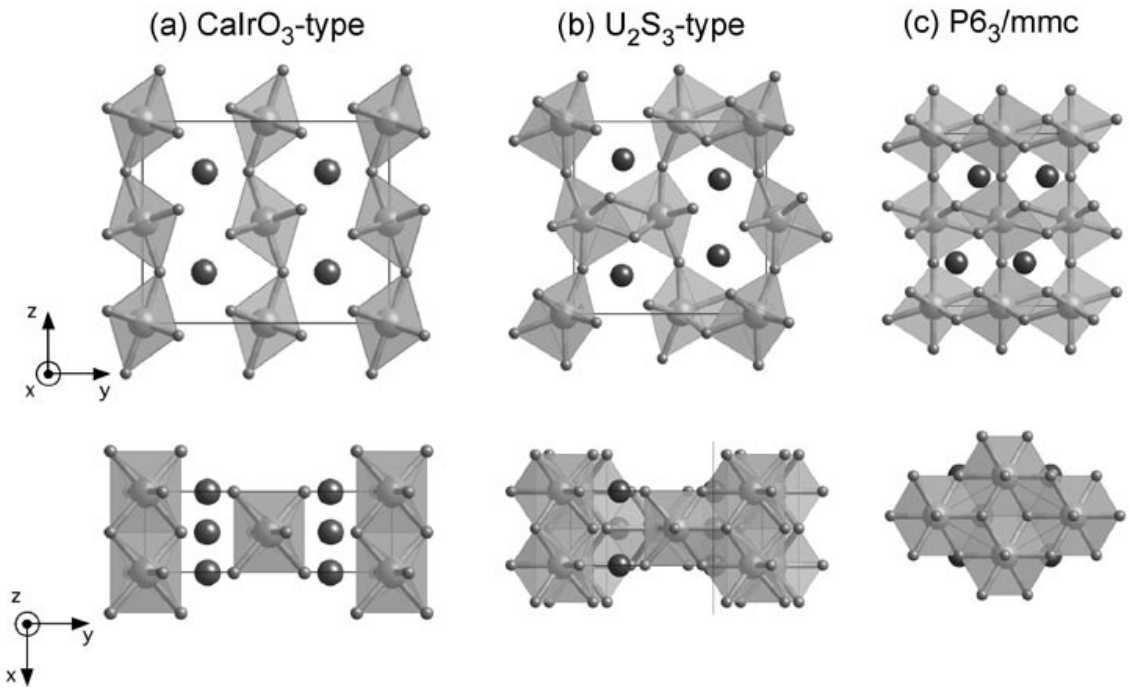

Figure 7. Structures of (a) $CaIrO_3$-type PPV and two possible candidates of post-PPV phases: (b) U_2S_3-type and (c) *P*6_3/*mmc* phases.

for post-PPV transitions in $NaMgF_3$ instead of the dissociation (Umemoto and Wentzcovitch 2006). Although they are metastable with respect to the dissociation products, the U_2S_3-type phase could actually be observed experimentally by compressing $CaIrO_3$-type $NaMgF_3$ at sufficiently low temperatures. The energy barrier for the dissociation is expected to be higher than that for the U_2S_3-type transition which is related to a soft mode. In addition, at low temperature, the phase boundaries for the dissociation and for the U_2S_3-type transition are close to each other. Recently Martin et al. (2006) reported diamond anvil cell experiments in *Cmcm* $NaMgF_3$ showing new X-ray diffraction peaks with increasing pressure. However, these peaks could not be

attributed only to a mixture of *Cmcm* and its dissociation products, NaF and MgF_2. The superposition of peaks seems to be considerable and the analysis of the published pattern is challenging and inconclusive; but, the new X-ray diffraction pattern may contain peaks related to the U_2S_3-type phase. In $MgSiO_3$, the static transition pressure to the U_2S_3-type phase is calculated to be beyond 1.6 TPa (Umemoto and Wentzcovitch 2006), which is considerably higher than the dissociation pressure of ~1 TPa. In nature these pressures are realized in the interior of the giant planets and exoplanets where temperatures are also expected to be very high, $10^{3.5}$~10^4 K. Since diffusion barriers are expected to be overcome in planetary time scales, dissociation into oxides is still the most likely pressure-induced transition in $CaIrO_3$-type $MgSiO_3$ in planetary interiors.

POST-POST-PEROVSKITE TRANSITION IN Al_2O_3

Two metastable candidate post-PPV structures—U_2S_3-type and $P6_3/mmc$ structures—were proposed for $NaMgF_3$ under pressure, but the most probable transition should be the dissociation into CsCl-type NaF and cotunnite-type MgF_2. However, sometimes dissociation is "forbidden." Al_2O_3 (alumina) is expected to undergo a non-dissociative post-PPV transition. Its highest-pressure phase identified experimentally so far, the $CaIrO_3$-type, has unlikely dissociation products, AlO and AlO_2. For Al_2O_3, two phase transitions have been established so far: corundum—Rh_2O_3(II)-type (Cynn et al. 1990; Marton and Cohen 1994; Thomson et al. 1996; Funamori and Jeanloz 1997; Mashimo et al. 2000; Lin et al. 2004) and Rh_2O_3(II)-type—$CaIrO_3$-type (PPV) (Caracas and Cohen 2005; Oganov and Ono 2005; Tsuchiya et al. 2005; Ono et al. 2006). Al_2O_3 is an important compound in high-pressure technology and geophysics. It is used as window material in shock-wave experiments (McQueen and Isaak 1990). The pressure dependence of the fluorescence line of ruby, Al_2O_3 doped with chromium, serves as a pressure-marker in diamond-anvil-cell experiments (Mao and Bell 1976; Chen and Silvera 1996). In Earth and planetary sciences, Al_2O_3 is a major chemical component in solid solution with $MgSiO_3$ garnet, PV, and PPV. The formation of these solid solutions with Al_2O_3 changes the properties, phase boundaries, electrical conductivity, oxidation state, and spin states of iron in $MgSiO_3$, (e.g., Wood and Rubie 1998; Xu et al. 1998; Zhang and Weidner 1999; Frost et al. 2004; Li et al. 2004; Taneno et al. 2005; Nishio-Hamane et al. 2007).

Static enthalpy calculations by Umemoto and Wentzcovitch (2008) clearly showed a post-PPV transition in Al_2O_3 to a U_2S_3-type phase (Fig. 8). The static transition pressure was predicted to be 373 (380) GPa by LDA (GGA). The $P6_3/mmc$ phase, another candidate for a post-PPV phase, was not found in Al_2O_3 up to 700 GPa. No phonon softening was observed both in the $CaIrO_3$-type and in the U_2S_3-type phases at least up to 700 GPa. These phases should be dynamically stable within this pressure range. Figure 9 shows the calculated phase boundaries of Al_2O_3. The post-PPV transition between the $CaIrO_3$-type and the U_2S_3-type phases has a positive Clapeyron slope, as in $NaMgF_3$.

It is interesting to compare calculated compression curves and those obtained by dynamic compression experiments. In a shock experiment to ~340 GPa, no direct evidence of phase transitions was noticed, although there was an atypical relationship between shock velocity (u_s) and particle velocity (u_p): $u_s = C + Su_p$ in which S (0.957) was unusually small, suggested a sluggish phase transformation (Erskine 1994). However, Figure 10 strongly suggests the presence of all three phases stable below 340 GPa in the raw data (Marsh 1980; Erskine 1994). With shock data alone, it is difficult to resolve phase transitions accompanied by small density changes comparable to the detectability limit.

The transition pressure to the U_2S_3-type polymorph of Al_2O_3 exceeds the pressure at the core-mantle boundary of the Earth (~135 GPa). Therefore the occurrence of U_2S_3-type Al_2O_3 should not alter the current views of the Earth's lower mantle. However, it might affect our

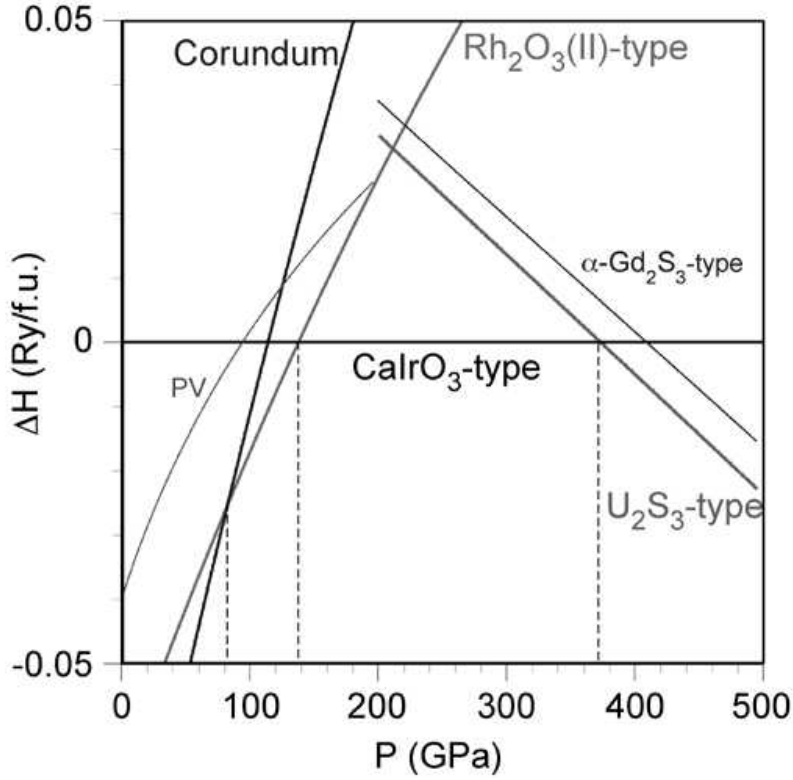

Figure 8. Relative static LDA enthalpies of Al_2O_3 polymorphs with respect to the $CaIrO_3$-type phase (Umemoto and Wentzcovitch 2008). Dashed vertical lines denote corundum—Rh_2O_3(II)-type, Rh_2O_3(II)-type—$CaIrO_3$-type, and $CaIrO_3$-type—U_2S_3-type transition pressures, respectively.

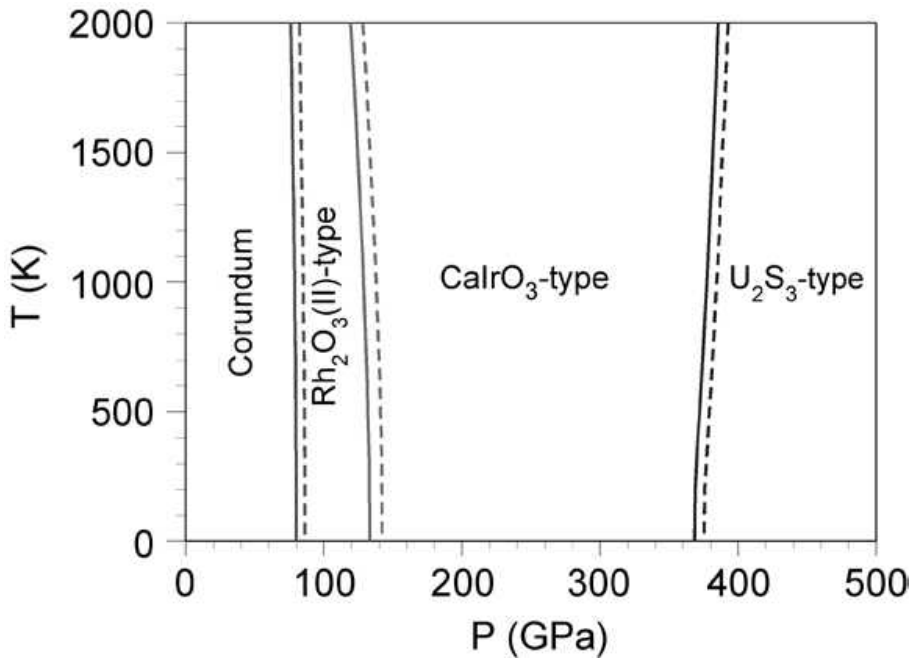

Figure 9. Calculated phase boundary in Al_2O_3 (Umemoto and Wentzcovitch 2008). Solid and dashed lines denote LDA and GGA phase boundaries.

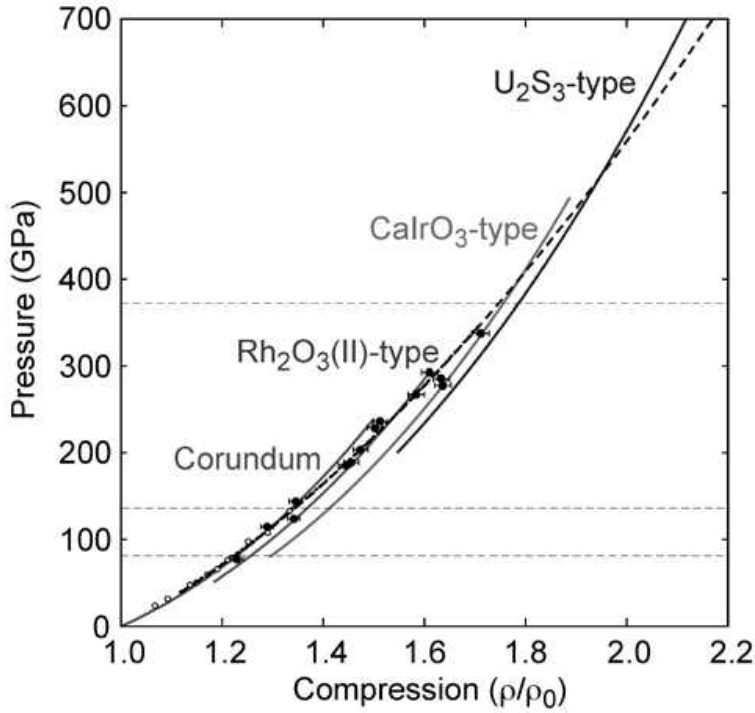

Figure 10. LDA static pressure vs compression (solid lines) (Umemoto and Wentzcovitch 2008). ρ is the calculated density of each phase and ρ_0 is that of corundum at 0 GPa. Horizontal dashed lines represent calculated transition pressures: 82 GPa for corumdum—Rh_2O_3(II)-type, 137 GPa for Rh_2O_3(II)-type—$CaIrO_3$-type, and 373 GPa for $CaIrO_3$-type—U_2S_3-type transitions. Experimental shock data are shown by black (Erskine 1994) and white circles (Marsh 1980). The black dashed line is a compression curve obtained by applying the Rankine-Hugoniot equations to a single linear fit to the Hugoniot data (Erskine 1994).

understanding of the rocky mantles of terrestrial exoplanets since it could change the solubility of Al_2O_3 in $CaIrO_3$-type $MgSiO_3$. The change in coordination number from 6 to 7 in the B site suggests that Al_2O_3 might ex-solve from $MgSiO_3$, in particular, from the smaller 6-fold B site occupied by silicon in the $CaIrO_3$-type structure. The ex-solution of Al_2O_3 could change electrical and thermal conductivities of the $CaIrO_3$-type solid solution, as the incorporation of Al_2O_3 changes the electrical conductivity of $MgSiO_3$ perovskite in presence of iron (Xu et al. 1998).

RARE-EARTH SESQUISULFIDES

Figure 11 shows crystal structures of rare-earth sesquisulfides, $RR'S_3$ (R, R′ = lanthanoid or actinoid), at 1000 °C and ambient pressure. In the $RR'S_3$ family of compounds, we find several structures (corumdum, $GdFeO_3$-type (i.e., perovskite), $CaIrO_3$-type, and U_2S_3-type structures) adopted by $MgSiO_3$ and Al_2O_3. In addition, $LaYbS_3$ adopts the $GdFeO_3$-type structure at high temperatures and the $CaIrO_3$-type structure at low temperatures (Rodier et al. 1983; Mitchell et al. 2004), being reminiscent of the post-perovskite transition in $MgSiO_3$ with a positive Clapeyron slope (Murakami et al. 2004; Oganov and Ono 2004; Tsuchiya et al. 2004). Therefore a close relationship is suggested between the multi-Mbar crystal chemistry of planet-forming minerals and that of rare-earth sesquisulfides. The relationship between $RR'S_3$ crystal structures and cation radii can be summarized as follows: the corundum structure occurs with small R and R′ radii (e.g., Yb_2S_3), the U_2S_3-type structure with large radii, and the $CaIrO_3$-type and the $GdFeO_3$-type structures with large R in the A site and small R′ in the B site (e.g., $NdYbS_3$ and $LaYbS_3$). In R_2S_3, coordination numbers increase with increasing cation radii (Fig. 12). This chemical-pressure effect produces a sequence of structures consistent with that

R

R′ \ R	(U)	La	Ce	Pr	Nd	Sm	Gd	Tb	Dy	(Y)	Ho	Er	Tm	Yb	Lu	(Sc)
(U)	η															
La		α	α_c	α_c	α_c	α_c	α_c	α_c	G	G	G	G	G	PV	PV	PV
Ce			α	α_c	α_c	α_c	α_c	α_c	α_1	G	G	G	G	PPV	PPV	PV
Pr				α	α_c	α_c	α_c	α_c	α_c	α_1	α_1	G	G	PPV	PPV	PV
Nd					α	α_c	α_c	α_c	α_c	α_1	α_1	α_1	G	PPV	PPV	PV
Sm						α	α_c	α_c	α_c	α_1	α_1	α_1	α_1	F	F	PV
Gd							α	α_c	α_c	x	x	x	F	F	F	PV
Tb								α	α_c	x	x	x	x	F	F	PV
Dy									α	δ_c	δ_c	δ_c	δ_c	δ_1	δ_1	PV
(Y)										δ	δ_c	δ_c	δ_c	δ_1	δ_1	PV
Ho											δ	δ_c	δ_c	δ_1	δ_1	PV
Er												δ	δ_c	δ_1	δ_1	PV
Tm													δ	δ_1	δ_1	-
Yb														ε	ε_c	-
Lu															ε	-

Figure 11. Polymorph of $RR'S_3$ compounds at 1000 °C (Flahaut 1979). Each symbol denotes the following structural types: η: U_2S_3-type, α: α-Gd_2S_3-type, δ: δ-Ho_2S_3-type, ε: corundum-type, F: $CeYb_3S_6$-type, G: $CeTmS_3$-type, PPV: $NdYbS_3$-type, i.e., $CaIrO_3$-type (see below), I: perovskite, α_c and δ_c: isomorphic solid solutions of the α or δ types, with compositions varying continuous from R_2S_3 to R'_2S_3, α_1 and δ_1: solid solutions of the α or δ types, with a limited solubilities, including the $RR'S_3$ composition, and x: mixture of phases with $RR'S_3$ composition. The $NdYbS_3$-type structure was first reported to have $B22_12$ symmetry which is a subgroup of the *Cmcm* group of the $CaIrO_3$-type structure (Flahaut 1979; Carré and Laruelle 1974). However, the $NdYbS_3$-type structure refined in the $B22_12$ symmetry is nearly indistinguishable from the $CaIrO_3$-type structure. The difference between them is very small. In the $B22_12$ $NdYbS_3$-type structure, the cation at the B site and one kind of sulfur are just slightly shifted from the 4a and 8f Wyckoff positions in the *Cmcm* $CaIrO_3$-type structure. A recent X-ray diffraction study suggested the $NdYbS_3$-type structure should have the *Cmcm* symmetry and be the same as the $CaIrO_3$-type structure (Mitchell et al. 2004).

induced by pressure in Al_2O_3. Therefore, *one might anticipate that rare-earth sesquisulfides are a set of low-pressure analogs of planet-forming silicates and oxides.* $RR'S_3$ structures that do not occur in $MgSiO_3$ and Al_2O_3, may also play an important role. In fact, Al_2O_3 in the Gd_2S_3-type structure, one of the major structures of $RR'S_3$ compounds, and the U_2S_3-type polymorph have very similar enthalpies (see Fig. 8). The Ho_2S_3-type structure is also one of the likely forms between corundum and the Gd_2S_3-type/U_2S_3-type phases, but for Al_2O_3, this phase has very high enthalpy and is energetically unstable.

M_2O_3 SESQUIOXIDES

In addition to rare-earth sesquisulfides, M_2O_3 sesquioxides (M = trivalent cations: group IIIB metals, gallium and indium, and *d*-transition metals) could be another set of low-pressure analogs of planet-forming sesquioxides, especially of Al_2O_3. Ga_2O_3 and Fe_2O_3 exhibit sequences of phase transitions similar to Al_2O_3: corundum—Rh_2O_3(II)-type—$CaIrO_3$-type phases (in Ga_2O_3, corundum phase is preceded by the β phase) (Shim and Duffy 2002; Ono et al. 2005; Ono and Ohishi 2005; Shim et al. 2009, Tsuchiya et al. 2007; Yusa et al. 2008a). The $CaIrO_3$-type structure occurs also in Mn_2O_3 (Santillán et al. 2006).

Caracas and Cohen (2007) performed a series of first-principles calculations of phase transitions in Al_2O_3, Ga_2O_3, Rh_2O_3, and In_2O_3. They showed that In_2O_3 should undergo the

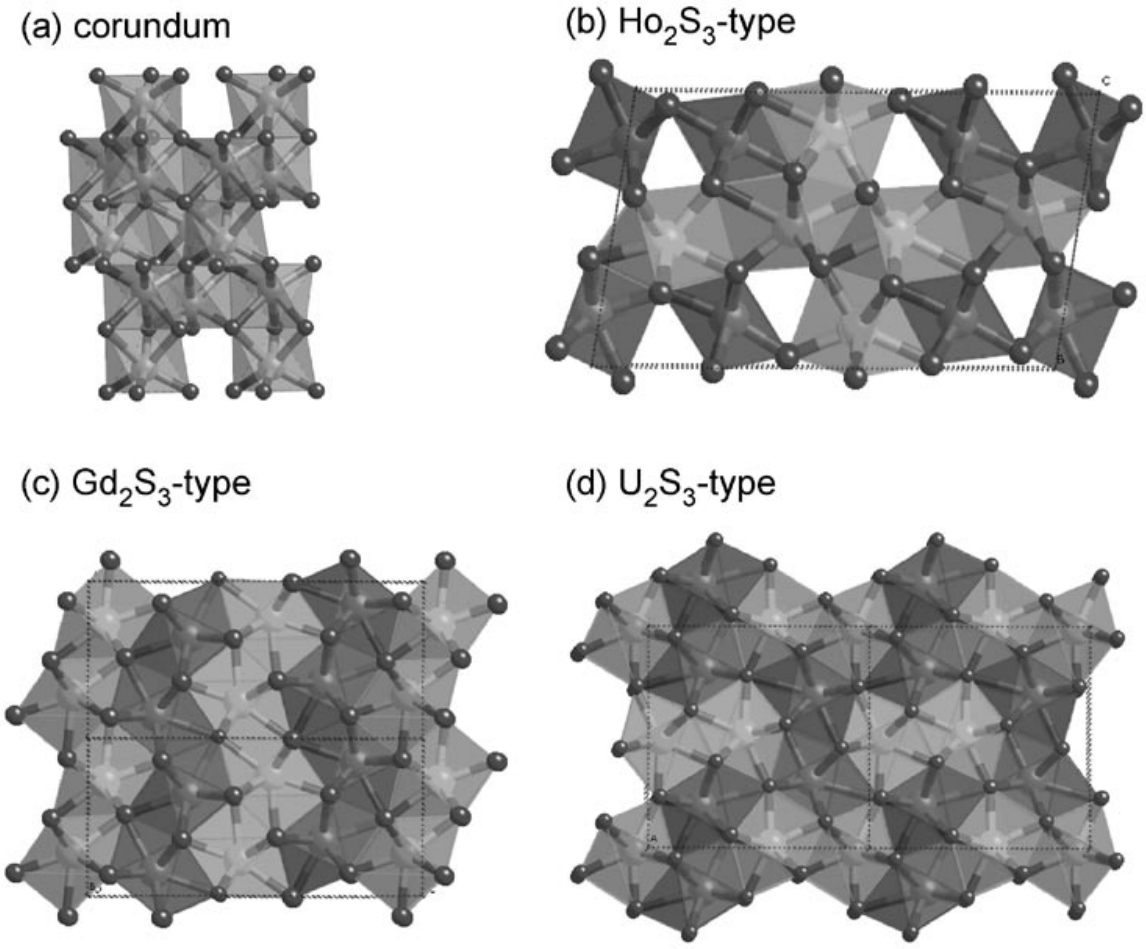

Figure 12. Crystal structures of R_2S_3 (R: lanthanoid or actinoid). The coordination numbers of cations are 6 in corundum, 6 and 7 in Ho_2S_3-type, 7 and 8(=7+1) in Gd_2S_3-type and U_2S_3-type structures.

Rh_2O_3(II)-type—$CaIrO_3$-type phase transition at a pressure as low as 47 GPa. In fact, In_2O_3 does not adopt quite exactly the $CaIrO_3$-type structure experimentally (Yusa et al. 2008b). The PPV transition pressures of Ga_2O_3 and Rh_2O_3 were estimated to be 136 GPa and ~360 GPa, respectively. This is contrary to expectations; The PPV transition pressure in Rh_2O_3 is expected to be lower than in Al_2O_3 and Ga_2O_3, since the ionic radius of rhodium (0.805 Å) is larger than those of aluminum (0.675 Å) and gallium (0.760 Å) (Shannon 1976). Results by Caracas and Cohen (2007) suggest the relationship between crystal structures in M_2O_3 and cation radii is not simple. Indeed, the sequence of phase transitions in M_2O_3 is very complex, as shown in Figure 13. This complexity indicates that *d* electrons may be an important factor for determination of crystal structures. Partially-filled *d* states have preferential orientations in space and should affect the positions of surrounding oxygens. Different *d* states filling factors in different cations may give rise to a variety of crystal structures. For Fe_2O_3, magnetization is also an important factor (Shim et al. 2009). In the case of rare-earth sesquisulfides, the occupation of *f* states varies, depending on the lanthanoid and actinoid atomic species. But the *f* states are quite localized and should hardly affect chemical bonding. Therefore the relationship between crystal structure and ionic radii in rare-earth sesquisulfides is rather simple.

The Gd_2S_3-type structure is a high-pressure form of In_2O_3 and Sc_2O_3 with relatively large ionic radii (Yusa et al. 2008b, 2009). But, in In_2O_3 and Sc_2O_3, the enthalpy differences between the Gd_2S_3-type and the U_2S_3-type phases were found to be very small. In some experimental conditions, both phases might coexist, as in Dy_2S_3 (Meetsma et al. 1991). Ti_2O_3 is very

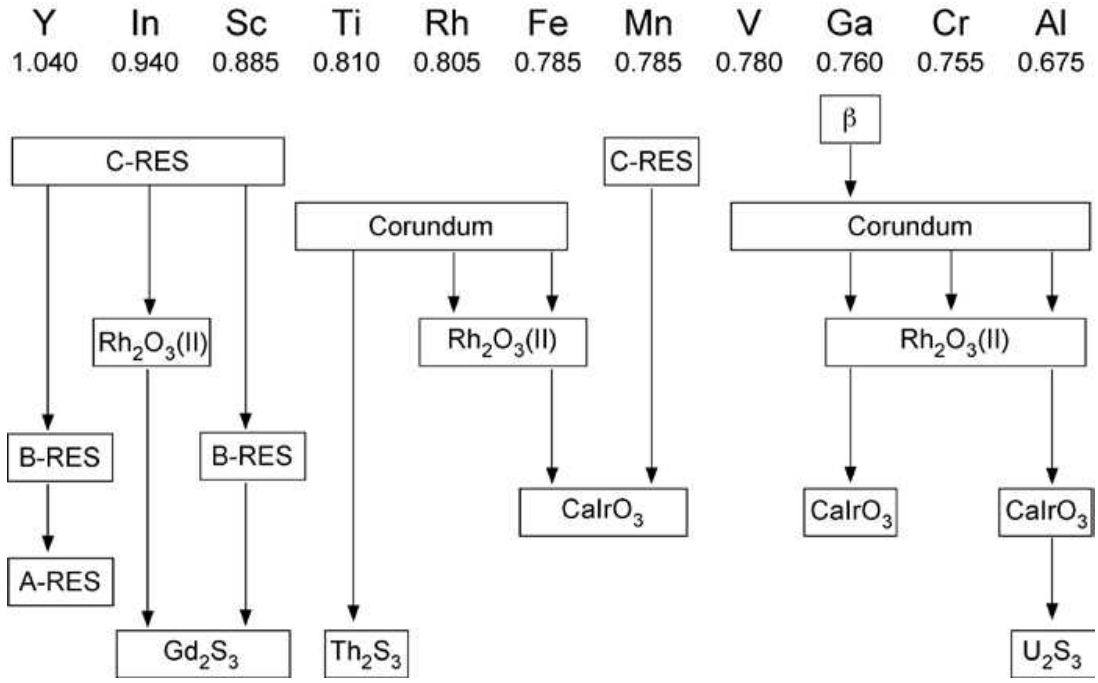

Figure 13. Summary of the sequence of phase transitions in M_2O_3. The numbers represent ionic radii of trivalent cations. Fe and Mn are assumed to be in the high-spin state (Shannon 1976). For simplicity, the monoclinic *I*2/*a* phase is omitted for V_2O_3 (Dernier and Marezio 1970) and Cr_2O_3 (Shim et al. 2004). This figure is based on the following references for each compound: Y_2O_3 (Atou et al. 1990; Husson et al. 1999; Wang et al. 2009), In_2O_3 (Yusa et al. 2008a,b), Sc_2O_3 (Yusa et al. 2009), Ti_2O_3 (Nishio-Hamane et al. 2009), Rh_2O_3 (Shannon and Prewitt 1970), Fe_2O_3 (Shim and Duffy 2002; Ono et al. 2005; Ono and Ohishi 2005; Shim et al. 2009), Mn_2O_3 (Santillán et al. 2006), Ga_2O_3 (Yusa et al. 2008), and Al_2O_3 (see the text).

interesting. It transforms directly from corundum to the Th_2S_3-type phase (Nishio-Hamane et al. 2009). The Th_2S_3-type structure is isostructural with U_2S_3. The symmetry of both structures is *Pnma*. The difference between them is the type of orthorhombic distortion: lattice constant $a < c$ in the Th_2S_3-type and $a > c$ in the U_2S_3-type structure. So far, no transition from the $CaIrO_3$-type phase has been identified experimentally in M_2O_3. For Ga_2O_3, Mn_2O_3, and Fe_2O_3, whose highest-pressure forms identified experimentally appears to be the $CaIrO_3$-type structure (Shim et al. 2009), we anticipate post-PPV phases with U_2S_3-type or Th_2S_3-type structures.

SUMMARY

Two post-post-perovskite transitions have been identified by first principles calculations: the dissociation of $MgSiO_3$ into CsCl-type MgO and cotunnite-type SiO_2 at ~1 TPa and the transition of Al_2O_3 to the U_2S_3-type phase at ~370 GPa. These transition pressures are currently very challenging for static compression experiments. $NaMgF_3$ may be a good low-pressure analog of $MgSiO_3$. We found a close relationship between the multi-Mbar crystal chemistry of planet-forming minerals and that of rare-earth sesquisulfides. Some of them may be used as low-pressure analogs of planet-forming minerals in the multi-Mbar range. In transition-metal sesquioxides, the Th_2S_3-type phase (very similar to U_2S_3-type) was discovered in Ti_2O_3, suggesting that some transition-metal sesquioxides could serve as low-pressure analog(s) of Al_2O_3. Finally, a new type of dissociation, $FeTiO_3$ perovskite into $(Fe_{1-\delta},Ti_\delta)O$ and $Fe_{1+\delta}Ti_{2-\delta}O_5$, has recently been reported (Wu et al. 2009). This finding suggests that solid solutions (probably with transition-metals) among dissociation products (and in parent phases) could complicate the transition mechanisms we have discussed in this chapter.

ACKNOWLEDGMENTS

Many parts of this article are based on a set of first-principles studies which we performed using the Quantum-ESPRESSO distribution (Giannozzi et al. 2009). These works were supported by NSF grants No. EAR-0135533, EAR-0230319, ITR-0428774 (Vlab), EAR-0757903, EAR-0635990, and ATM-0428774 (Vlab).

REFERENCES

Atou T, Kusaba K, Fukuoka K, Kikumi M (1990) Shock-induced phase transition of M_2O_3 (M=Sc, Y, Sm, Gd, and In)-type compounds. J Solid State Chem 89:378-384

Baroni S, de Gironcoli S, Dal Corso A, Giannozzi P (2001) Phonons and related crystal properties from density-functional perturbation theory. Rev Mod Phys 73:515-562

Caracas R, Cohen RE (2005) Prediction of a new phase transition in Al_2O_3 at high pressures. Geophys Res Lett 32:L06303

Caracas R, Cohen RE (2007) Post-perovskite phase in selected sesquioxides from density-functional calculations. Phys Rev B 76:184101

Carré PD, Laruelle P (1974) Structure Cristalline du Sulfure de Néodyme et d'Ytterbium, $NdYbS_3$. Acta Cryst B30:952-954

Ceperley DM, Alder BJ (1980) Ground state of the electron gas by a stochastic method. Phys Rev Lett 45:566-569

Chen NH, Silvera IF (1996) Excitation of ruby fluorescence at multimegabar pressures. Rev Sci Instrum 67:4275-4278

Cynn H, Isaak DG, Cohen RE, Nicol MF, Anderson OL (1990) A high-pressure phase transition of corundum predicted by the potential induced breathing model. Am Mineral 75:439-442

Dernier PD, Marezio M (1970) Crystal structure of the low-temperature antiferromagnetic phase of V_2O_3. Phys Rev B 2:3771-3776

Erskine D (1994) High pressure Hugoniot of sapphire. *In*: High Pressure Science and Technology—1993. Schidt SC, Shaner JW, Samara GA, Ross M (eds) AIP Press, New York, p 141-143

Flahaut J (1979) Sulfides, selenides, and tellurides. *In*: Handbook on the Physics and Chemistry of Rare-Earths. Gschneidner KA Jr., Eyring LR (eds) North-Holland, Amsterdam, New York, Oxford. 4:1-88

Frost DJ, Liebske C, Langenhorst F, McCammon CA, Trannes RG, Rubie DC (2004) Experimental evidence for the existence of iron-rich metal in the Earth's lower mantle. Nature 428:409-412

Funamori N, Jeanloz R (1997) High-pressure transformation of Al_2O_3. Science 278:1109-1111

Giannozzi P, de Gironcoli S, Pavone P, Baroni S (1991) *Ab initio* calculation of phonon dispersions in semiconductors. Phys Rev B 43:7231-7242

Giannozzi P, Baroni S, Bonini N, Calandra M, Car R, Cavazzoni C, Ceresoli D, Chiarotti GL, Cococcioni M, Dabo I, Dal Corso A, de Gironcoli S, Fabris S, Fratesi G, Gebauer R, Gerstmann U, Gougoussis C, Kokalj A, Lazzeri M, Martin-Samos L, Marzari N, Mauri F, Mazzarello R, Paolini S, Pasquarello A, Paulatto L, Sbraccia C, Scandolo S, Sclauzero G, Seitsonen AP, Smogunov A, Umari P, Wentzcovitch RM (2009) Quantum ESPRESSO: a modular and open-source software project for quantum simulations of materials. J Phys Condens Matter 21:395502

Guillot T (2004) Probing the giant planet. Phys Today 57 (4):63-69

Haines J, Leger JM, Gorelli F, Klug DD, Tse JS, Li ZQ (2001) X-ray diffraction and theoretical studies of the high-pressure structures and phase transitions in magnesium fluoride. Phys Rev B 64:134130

Hirose K, Fujita Y (2005) Clapeyron slope of the post-perovskite phase transition in $CaIrO_3$. Geophys Res Lett 32:L13313-13316

Hirose K, Kawamura K, Ohishi Y, Tateno S, Sata N (2005) Stability and equation of state of $MgGeO_3$ post-perovskite phase. Am Mineral 90:262-265

Hohenberg P, Kohn W (1964) Inhomogeneous electron gas. Phys Rev 136:B864-B871

Husson E, Proust C, Gillet P, Itié JP (1999) Phase transitions in yttrium oxide at high pressure studied by Raman spectroscopy. Mater Res Bull 34:2085-2092

Hustoft J, Catalli K, Shim SH, Kubo A, Prakapenka VB, Kunz M (2008) Equation of state of $NaMgF_3$ postperovskite: Implication for the seismic velocity changes in the D'' region. Geophys Res Lett 35:L10309

Hyde BG, Andersson S, Bakker M, Plug CM, O'Keeffe M (1979) The (twin) composition plane as an extended defect and structure-building entity in crystals. Prog Solid St Chem 12: 273-327

Hyde BG, Andersson S (1989) Inorganic Crystal Structures. Wiley, New York

Kohn W, LJ Sham (1965) Self-consistent equations including exchange and correlation effects. Phys Rev 140:A1133-A1138

Kubo A, Kiefer B, Shen G, Prakaoebja VB, Cava RJ, Duffy TS (2006) Stability and equation of state of the post-perovskite phase in $MgGeO_3$ to 2 Mbar. Geophys Res Lett 33:L12S12-12S15

Kubo A, Kiefer B, Shim SH, Shen G, Prakapenka VB, Duffy T (2008) Rietveld structure refinement of $MgGeO_3$ post-perovskite phase to 1 Mbar. Am Mineral 93:965-976

Li J, Struzhkin VV, Mao HK, Shu J, Hemley RJ, Fei Y, Mysen B, Dera P, Prakapenka V, Shen G (2004) Electronic spin state of iron in lower mantle perovskite. Proc Nat Acad Sci USA 101:14027-14030

Lin JF, Degtyareva O, Prewitt CT, Dera P, Sata N, Gregoryanz E, Mao HK, Hemley RJ (2004) Crystal structure of a high-pressure/high-temperature phase of alumina by in situ X-ray diffraction. Nat Mater 3:390-393

Liu HZ, Chen J, Hu J, Martin CD, Weidner DJ, Häusermann D, Mao HK (2005) Octahedral tilting evolution and phase transition in orthorhombic $NaMgF_3$ perovskite under pressure. Geophys Res Lett 32:L04304-04307

Mao HK, Bell PM (1976) High pressure physics: I Megabar in ruby R1 static pressure scale. Science 191:851-852

Marsh S (1980) LASL Shock Hugoniot Data. Univ of California Press, Berkeley, p. 260

Martin CD, Crichton WA, Liu H, Prakapenka V, Chen J, Parise JB (2006) Phase transitions and compressibility of $NaMgF_3$ (neighborite) in perovskite- and post-perovskite-related structures. Geophys Res Lett 33:L11305

Marton FC, Cohen RE (1994) Prediction of a high-pressure phase transition in Al_2O_3. Am Mineral 79:789-792

Mashimo T, Tsumoto K, Nakamura K, Noguchi Y, Fukuoka K, Syono Y (2000) High-pressure phase transformation of corundum (α-Al_2O_3) observed under shock compression. Geophys Res Lett 27:2021-2024

McQueen RG, Isaak DG (1990) Characterizing windows for shock-wave radiation studies. J Geophys Res 95 (B13):21753-21765

Meetsma A, Wiegers GA, Haange RJ, de Boer JL, Boom G (1991) Structure of two modifications of dysprosium sesquisulfide, Dy_2S_3. Acta Crystallogr C47:2287-2291

Mehl MJ, Cohen RE, Krakauer H (1988) Linearized augmented plane wave electronic structure calculations for MgO and CaO. J Geophys Res 93(B7):8009-8022

Mermin ND (1965) Thermal properties of the inhomogeneous electron gas. Phys Rev 137:A1441-A1443

Mitchell K, Somers RC, Huang FQ, Ibers JA (2004) Syntheses, structure, and magnetic properties of several LnYbQ3 chalcogenides, Q=S, Se. J Solid State Chem 177:709-713

Murakami M, Hirose K, Kawamura K, Sata N, Ohishi Y (2004) Post-perovskite transition in $MgSiO_3$. Science 304:855-858

Nishio-Hamane D, Fujino K, Seto Y, Nagai T (2007) Effect of the incorporation of $FeAlO_3$ into $MgSiO_3$ perovskite on the post-perovskite transition. Geophys Res Lett 34:L12307

Nishio-Hamane D, Katagiri M, Niwa K, Sano-Furukawa A, Okada T, Yagi T (2009) A new high-pressure polymorph of Ti_2O_3: implication for high-pressure phase transition in sesquioxides. High Pressure Res 29:379-388

Oganov AR, Gillan MJ, Price GD (2003) *Ab initio* lattice dynamics and structural stability of MgO. J Chem Phys 118:10174-10182

Oganov AR, Ono S (2004) Theoretical and experimental evidence for a post-perovskite phase of $MgSiO_3$ in Earth's D″ layer. Nature 430:445-448

Oganov AR, Gillan MJ, Price GD (2005a) Structural stability of silica at high pressures and temperatures. Phys Rev B 71:064104

Oganov AR, Ono S (2005) The high-pressure phase of alumina and implications for Earth's D″ layer. Proc Nat Acad Sci USA 102:10828-10831

Ono S, Funakoshi K, Ohishi Y, Takahashi E (2005) *In situ* x-ray observation of the phase transformation of Fe_2O_3. J Phys Condens Matt 17:267-276

Ono S, Ohishi Y(2005) *In situ* X-ray observation of phase transformation in Fe_2O_3 at high pressures and high temperatures. J Phys Chem Solids 66:1714-1720

Ono S, Oganov AR, Koyama T, Shimizu H (2006) Stability and compressibility of the high-pressure phases of Al_2O_3 up to 200 GPa: Implications for the electrical conductivity of the base of the lower mantle. Earth Planet Sci Lett 246:326-335

Perdew JP, Zunger A (1981) Self-interaction to density-functional approximations for many-electron systems. Phys Rev B 23:5048-5079

Perdew JP, Burke K, Ernzerhof M (1996) Generalized gradient approximation made simple. Phys Rev Lett 77:3865-3868

Rivera EJ, Lissauer JJ, Butler RP, Marcy GW, Vogt SS, Fischer DA, Brown TM, Laughlin G, Henry GW (2005) A similar to 7.5 $M_\oplus$ plus planet orbiting the nearby star, GJ 876. Astrophys J 634:625-640

Rodier PN, Julien R, Tien V (1983) Polymorphisme de $LaYbS_3$. Affinement des structures des deux varieties. Acta Crystallogr C39:670-673

Ross NL, Navrotsky A (1988) Study of the $MgGeO_3$ polymorphs (orthopyroxene, clinopyroxene, and ilmenite structures) by calorimetry, spectroscopy, and phase equilibria. Am Mineral 73:1355-1365

Santillán J, Shim SH, Shen G, Prakapenka VB (2006) High-pressure phase transition in Mn_2O_3: Application for the crystal structure and preferred orientation of the $CaIrO_3$ type. Geophys Res Lett 33:L15307

Sato B, Fischer DA, Henry GW, Laughlin G, Butler RP, Marcy GW, Vogt SS, Bodenheimer P, Ida S, Toyota E, Wolf A, Valenti JA, Boyd LJ, Johnson JA, Wright JT, Ammons M, Robinson S, Strader J, McCarthy C, Tah KL, Minnti D (2005) The N2K consortium. II. A transiting hot Saturn around HD 149026 with a large dense core. Astrophys J 633:465-473

Shannon RD, Prewitt CT (1970) Synthesis and structure of a new high-pressure form of Rh_2O_3. J Solid State Chem 2:134-136

Shannon RD (1976) Revised effective ionic radii and systematic studies of interatomic distances in halides and chalcogenides. Acta Cryst A32:751-767

Shim SH, Duffy TS (2002) Raman spectroscopy of Fe_2O_3 to 62 GPa. Am Mineral 87:318-326

Shim SH, Duffy TS, Jeanloz R, Yoo CS, Iota V (2004) Raman spectroscopy and x-ray diffraction of phase transitions in Cr_2O_3 to 61 GPa. Phys Rev B 69:144107

Shim SH, Bengtson A, Morgan D, Sturhahn W, Catalli K, Zhao J, Lerche M, Prakapenka V (2009) Electronic and magnetic structures of the postperovskite-type Fe_2O_3 and implications for planetary magnetic records and deep interiors. Proc Nat Acad Sci USA 106:5508-5512

Sun T, Umemoto K, Wu Z, Zhen JC, Wentzcovitch RM (2008) Lattice dynamics and thermal equation of stated of platinum. Phys Rev B 78:024304

Tackley P (1995) On the penetration of an endothermic phase transition by upwellings and downwellings. J Geophys Res 100 (B8):15477-15488

Tateno S, Hirose K, Sata N, Ohishi Y (2005) Phase relations in $Mg_3Al_2Si_3O_{12}$ to 180 GPa: Effect of Al on post-perovskite phase transition. Geophys Res Lett 32:L15306

Thomson KT, Wentzcovitch RM, Bukowinski MST (1996) Polymorphs of alumina predicted by first principles: Putting pressure on the ruby pressure scale. Science 274:1880-1882

Tsuchiya T, Tsuchiya J, Umemoto K, Wentzcovitch RM (2004) Phase transition in $MgSiO_3$ perovskite in the earth's lower mantle. Earth Planet Sci Lett 224:241-248

Tsuchiya J, Tsuchiya T, Wentzcovitch RM (2005) Transition from the Rh_2O_3(II)-to-$CaIrO_3$ structure and the high-pressure-temperature phase diagram of alumina. Phys Rev B 72:020103(R)

Tsuchiya T, Tsuchiya J (2006) New high-pressure phase relations in $CaSnO_3$. Am Mineral 91:1879-1887

Tsuchiya T, Tsuchiya J (2007) Structure and elasticity of *Cmcm* $CaIrO_3$ and their pressure dependences: *Ab initio* calculations. Phys Rev B 76:144119

Tsuchiya T, Yusa H, Tsuchiya J (2007) Post-Rh_2O_3(II) transition and the high pressure-temperature phase diagram of Gallia: A first-principles and x-ray diffraction study. Phys Rev B 76:174108

Umemoto K, Wentzcovitch RM (2006) Potential ultrahigh pressure polymorphs of ABX_3-type compounds. Phys Rev B 74:224105

Umemoto K, Wentzcovitch RM (2008) Prediction of an U_2S_3-type polymorph of Al_2O_3 at 3.7 Mbar. Proc Nat Acad Sci USA 105:6526-6530

Umemoto K, Wetnzcovitch RM, Allen PB (2006a) Dissociation of $MgSiO_3$ in the cores of gas giants and terrestrial exoplanets. Science 311:983-986

Umemoto K, Wentzcovitch RM, Weidner DJ, Parise JB (2006b) $NaMgF_3$: A low-pressure analog of $MgSiO_3$. Geophys Res Lett 33:L15304

Valencia D, O'Connell RJ, Sasselov D (2006) Internal structure of massive terrestrial planets. Icarus 181:545-554

Vanderbilt D (1990) Soft self-consistent pseudopotentials in a generalized eigenvalue formalism. Phys Rev B 41:7892-7895(R)

Wallace D (1972) Thermodynamics of Crystals. John Wiley, Hoboken, NJ

Wang L, Pan Y, Ding Y, Yang Y, Yang W, Mao WL, Sinogeikin SV, Meng Y, Shen G, Mao HK (2009) High-pressure induced phase transition of Y_2O_3 and Y_2O_3:Eu^{3+}. Appl Phys Lett 94:061921

Weinstein SA (1995) The effects of a deep mantle endothermic phase change on the structure of thermal convection in silicate planets. J Geophys Res 100(E6):11719-11728

Wentzcovitch RM (1991) Invariant molecular-dynamics approach to structural phase transitions. Phys Rev B 44:2358-2361

Wentzcovitch RM, Martins JL, Allen PB (1992) Energy versus free energy in first principles calculations. Phys Rev B 45:11372-11374

Wentzcovitch RM, Martins JL, Price GD (1993) *Ab Initio* molecular dynamics with variable cell shape: application to $MgSiO_3$. Phys Rev Lett 70:3947-3950

Wentzcovitch RM, Yu YG, Wu Z (2010) Thermodynamic properties and phase relations in mantle minerals investigated by first principles quasiharmonic theory. Rev Mineral Geochem 71:59-98

Wood BJ, Rubie DC (1998) The effect of alumina on phase transformations at the 660-kilometer discontinuity from Fe-Mg partitioning experiments. Science 273:1522-1524

Wu X, Steinle-Neumann G, Narygina O, Kantor I, McCammon C, Prakapenka V, Swamy V, Dubrovinsky L (2009) High-pressure behavior of perovskite: $FeTiO_3$ dissociation into $(Fe_{1-\delta},Ti_{\delta})O$ and $Fe_{1+\delta}Ti_{2-\delta}O_5$. Phys Rev Lett 103:065503

Wu Z, Umemoto K, Wu A, Zhen JC, Wentzcovitch RM (2008) P-V-T relations in MgO; an ultra-high pressure scale for planetary sciences applications. J Geophys Res 113:B06204

Xu Y, McCammon C, Poe BT (1998) The effect of alumina on the electrical conductivity of silicate perovskite. Science 282:922-924

Yagi T, Suzuki T, Akimoto S (1983) New high-pressure polymorphs ion sodium halides. J Phys Chem Solids 44:135-140

Yusa H, Tsuchiya T, Sata N, Ohishi Y (2008a) Rh_2O_3(II)-type structures in Ga_2O_3 and In_2O_3 under high pressure: Experiment and theory. Phys Rev B 77:064107

Yusa H, Tsuchiya T, Tsuchiya J, Sata N, Ohishi Y (2008b) α-Gd_2S_3-type structure in In_2O_3: Experiments and theoretical confirmation of a high-pressure polymorph in sesquioxide. Phys Rev B 78:092107

Yusa H, Tsuchiya T, Sata N, Ohishi Y (2009) High-pressure phase transition to the Gd_2S_3 structure in Sc_2O_3: a new trend in dense structures in sesquioxides. Inorg Chem 48:7537-7543

Zhang J, Weidner DJ (1999) Thermal Equation of state of aluminum-enriched silicate perovskite. Science 284:782-784

Zhao Y, Weidner DJ, Ko J, Leinenweber K, Liu X, Li B, Meng Y, Pacalo REG, Vaughan MT, Wang Y, Yeganeh-Haeri A (1994) Perovskite at high P-T conditions: An in situ synchrotron X ray diffraction study of $NaMgF_3$ perovskite. J Geophys Res 99(B2):2871-2885